Journal of Quaternary Science

Lateglacial rock-slope failures in NW Ireland: age, causes and implications

Journal:	*Journal of Quaternary Science*
Manuscript ID:	JQS-13-0085.R1
Wiley - Manuscript type:	Research Article
Date Submitted by the Author:	n/a
Complete List of Authors:	Ballantyne, Colin; University of St Andrews, Geography and Geoscences Wilson, Peter; University of Ulster, School of Environmental Sciences schnabel, christoph Xu, Sheng; Scottish Universities Environmental Research Centre,
Keywords:	10Be exposure dating, rock-slope failure, paraglacial, stress release, palaeoseismicity

Lateglacial rock slope failures in NW Ireland: age, causes and implications

COLIN K. BALLANTYNE[1*], PETER WILSON[2], CHRISTOPH SCHNABEL[3] and SHENG XU[3]

[1] School of Geography and Geosciences, University of St. Andrews, St. Andrews, UK
[2] Environmental Sciences Research Institute, School of Environmental Sciences, University of Ulster, Cromore Road, Coleraine, UK
[3] NERC Cosmogenic Isotope Facility at SUERC, Scottish Enterprise Technology Park, Rankine Avenue, East Kilbride, Glasgow, UK

ABSTRACT: Nine postglacial quartzite rock slope failures (RSFs) in NW Ireland were dated using cosmogenic ^{10}Be. Weighted mean RSF ages range from 17.7 ± 0.9 ka to 12.5 ± 0.7 ka or 16.6 ± 0.7 ka to 11.7 ± 0.5 ka, depending on assumed ^{10}Be production rate. All dated RSFs occurred within ~5000 years following ice-sheet deglaciation at ~17.4ka (~16.3 ka) and all but two occurred within 2000 years after deglaciation. The timing of RSFs rules out glacial 'debuttressing', permafrost degradation and enhanced deglacial cleft-water pressures as triggers of failure in most cases. We infer that paraglacial stress release and associated fracture propagation were critical in reducing rock masses to critical stability, though earthquakes caused by Lateglacial glacio-isostatic rebound and/or release of stored tectonic stresses may have triggered failure in some or all cases. In conjunction with data from related studies, our results imply that most undated RSFs outside the limit of Younger Dryas glaciation in the British Isles are of Lateglacial age, and that numerous Lateglacial RSFs occurred inside these limits, with subsequent removal of debris by glaciers. They support the view that paraglacial RSF activity in tectonically-stable intraplate terrains was concentrated within a few millennia following deglaciation.

KEYWORDS: ^{10}Be exposure dating; rock slope failure; paraglacial; stress release; palaeoseismicity.

*Correspondence to: Colin Ballantyne, as above.
Email: ckb@st-and.ac.uk

Introduction

Large relict rock slope failures (RSFs) in the form of rockslides, rock avalanches, major rockfalls and in situ slope deformations are common in many formerly-glaciated mountain areas (Korup *et al.,* 2007). Such RSFs are commonly described as 'paraglacial', implying that glaciation and deglaciation have been instrumental in preconditioning failure (Ballantyne, 2002; McColl, 2012). Steepening of valley-side slopes by glacial erosion has long been identified as a potential cause of RSFs, and more recently attention has focused on the role of differential loading by glacier ice and subsequent unloading during deglaciation in reducing rock-slope stability. Glacial loading and unloading alters the state of stress within rock masses, potentially reducing them to a state of conditional stability whereby failure is triggered by such factors as removal of supporting ice during deglaciation ('debuttressing'), seismic activity, thaw of permafrost ice in rock joints, high cleft-water pressures, or progressive rock-slope weakening by incremental gravity-driven deformation, brittle fracture through rock bridges or chemical weathering (e.g. Eberhardt *et al.,* 2004; Bigot-Cormier *et al.*, 2005; Gruber and Haeberli, 2007; Cossart *et al.,* 2008; Haeberli *et al.,* 2008; Brideau *et al.,* 2009; Allen *et al.,* 2010; Gugliemi & Cappa, 2010; Sanchez *et al.,* 2010; Leith *et al.,* 2011; Yamasaki and Chigira, 2011; Krautblatter *et al.,* 2012, 2013; McColl, 2012).

Surface exposure dating using cosmogenic isotopes is routinely employed to establish the age of individual RSFs in glaciated steeplands, allowing inferences to be made concerning triggering factors (e.g. Mitchell *et al.,* 2007; Cossart *et al.,* 2008; Hermanns and Schellenberger, 2008; Hormes *et al.,* 2008; Antinao and Gosse, 2009; Dortch *et al.,* 2009; Ivy-Ochs *et al.,* 2009; Shroder *et al.,* 2011; Ivy-Ochs and Schaller, 2010; Sanchez *et al.,* 2010; Stock and Uhrhammer, 2010; Hermanns and Niedermann, 2011; Hewitt *et al.,* 2011; Penna *et al.,* 2011). Few studies, however, have attempted to identify the temporal pattern of postglacial RSF activity, and specifically how this changes with time elapsed since deglaciation.

Several authors have suggested that RSF frequency peaks immediately after ice retreat and declines abruptly or gradually thereafter (e.g. Abele, 1974; Cruden and Hu, 1993; Soldati *et al.,* 2004). Numerous documented cases of RSFs following recent deglaciation (Evans and Clague, 1994; Ballantyne, 2002; Arsenault and Meigs, 2005; Allen *et al.,* 2010) provide some support for this view, but the evidence relating to the timing of RSFs following Late Pleistocene glaciation suggests a more complex temporal pattern. From the seismic stratigraphy of rock avalanche deposits in Norwegian fjords, Blikra *et al.* (2006) detected a peak of RSF activity during deglaciation, but also another late in the Holocene. Similarly, ^{14}C-dated RSFs in the Austrian Alps suggest an early Holocene (~10.5 ka to ~9.4 ka) peak in activity, but also a secondary peak several millennia later (Prager *et al.*, 2008). From the seismic stratigraphy of rock avalanche deposits in Inner Storfjorden (western Norway) Longva *et al.* (2009) inferred that ~89% of the volume of postglacial RSF runout represents deposition during deglaciation (~14.7 ka to ~11.7 ka), but that rock avalanche frequency apparently peaked later, in the early Holocene (~11.7 ka to ~10 ka). Robust evidence for relatively rapid response of glacially-conditioned RSFs is provided by Fauqué *et al.* (2009), who constrained the ages of very large postglacial rock avalanches in the southern Andes using a combination of radiocarbon and cosmogenic ^{36}Cl dating; apart from one anomalously old date, their 11 RSF ages all fall within the Lateglacial and early Holocene (~13.9 ka to ~8.2 ka).

Equally, however, many RSFs have been shown to have occurred several millennia after Late Pleistocene deglaciation, particularly in active orogenic belts (Hewitt *et al.,* 2008 and references therein). A global dataset of 32 dated RSFs in formerly glaciated environments compiled by McColl (2012) depicts a clustering in the early Holocene (10–8 ka), but also suggests that many postglacial RSFs occurred much later.

Within the British Isles, exposure ages obtained for seven RSF sites in the Highlands of Scotland also suggest a complex pattern of response, with some occurring during the Lateglacial period (Ballantyne and Stone, 2009; Ballantyne *et al.,* 2009) but others during the mid-Holocene (Ballantyne *et al.,* 1998; Ballantyne and Stone, 2004). Collation and recalibration of these ages and dating of ten additional RSF sites in the same region enabled Ballantyne and Stone (2013) to reconstruct the temporal pattern of 17 RSFs based on 47 surface exposure ages. Ten RSF sites produced Lateglacial and early Holocene (> 9.8 ka) ages, and the ages for the remaining seven sites are scattered throughout the Holocene without significant clustering. By comparing RSF ages with the approximate timing of deglaciation at each site, they showed that their dated RSFs fall into two groups: ‘rapid response’ RSFs that failed during or within a millennium after deglaciation (seven sites) and ‘delayed response’ RSFs that failed at various times throughout the Lateglacial and Holocene. Their dated RSFs, however, include not only sites deglaciated prior to ~14.0 ka as the last British-Irish Ice Sheet retreated, but also sites deglaciated much later following reoccupation of Highland valleys by glaciers during the Younger Dryas Stade (YDS) of ~12.9–11.7 ka. Additionally, their dated RSFs occurred on a wide range of lithologies, so geological controls on the timing of failure are not taken into account.

The aims of the research reported here are: (1) to establish the temporal pattern of nine RSFs seated on a uniform lithology (quartzite) within a relatively small area (County Donegal, NW Ireland) that was deglaciated during retreat of the last British-Irish Ice Sheet and not subsequently reoccupied by glacier ice; and (2) to assess the implications of this pattern in terms of triggering mechanisms. Our research tests four competing hypotheses: (1) that failure represents a rapid and immediate response to deglaciation; (2) that RSF activity peaked over a few millennia in the Lateglacial and early Holocene, as suggested by several previous studies (Blikra *et al.,* 2006; Prager *et al.,* 2008; Fauqué *et al.,* 2009; Longva *et al.,* 2009); (3) that the timing of failure corresponds to the 'rapid plus delayed' response pattern identified by Ballantyne and Stone (2013) for RSFs in the Scottish Highlands; and (4) that the timing of failure extends throughout the postglacial period, without significant clustering.

The Donegal mountains

The principal quartzite mountains of NW Donegal form a chain of summits that extends northeastwards from Errigal (751 m) to Muckish (666 m) and includes the intervening summits of Mackoght (555 m), Aghla More (584 m), Aghla Beg (564 m) and Ardloughnabrackbaddy (603 m; Fig. 1). We obtained samples for ^{10}Be surface exposure dating from eight RSF sites in this area, as well as from a single RSF on the outlying peak of Slieve League (595 m), 57 km southwest of Errigal. All are underlain by massive, well-bedded quartzite of Dalradian age (Long and McConnell, 1997, 1999).

During the Last Glacial Maximum (~26–21 ka), the last British-Irish Ice Sheet extended to the Atlantic shelf edge, ~90 km west of the present-day Donegal coastline (Ó Cofaigh *et al.,* 2012), implying that all summits in the region were buried under several hundred metres of ice. Striae, roches moutonnées and erratics indicate northerly to northwesterly ice movement across the Errigal-Muckish Chain, and westerly to southwesterly ice movement around Slieve League (Charlesworth, 1926; Ballantyne *et* *al.,* 2007). Granite erratics and/or ice-scoured bedrock occur on all the lower summits (Wilson, 1993) indicating over-running by erosive warm-based ice, though summit blockfields on Errigal, Muckish and Slieve League suggest limited modification by glacier ice and former occupation by cold-based ice that was frozen to the underlying substrate (Ballantyne *et al.,* 2007; Fabel *et al.,* 2012). ^{10}Be exposure ages reported by Clark *et al.* (2009) for samples obtained from boulders on a moraine at Bloody Foreland (Fig. 1) imply that NW Donegal had emerged from under the retreating ice-sheet margin by 19.3 ± 1.2 ka, and a ^{10}Be-dated sample from bedrock at Glencolumbkille near Malin Beg (recalibrated from data in Ballantyne *et al.* (2007) using the LL local ^{10}Be production rate; see below) suggests that the westernmost headland of Donegal emerged from the ice sheet after 19.3 ± 1.0 ka. Evidence for glacial reoccupation of the Donegal mountains during the YDS is limited to the Derryveagh Mountains (Wilson, 2004a), outside the area of the sampled RSFs.

Wilson (1990a, 1990b, 1993) mapped ten deposits of coarse rock debris that extend outwards from the foot of talus accumulations in the Errigal-Muckish mountains (Fig. 1). The largest of these take the form broad lobes of hummocky rock debris, often aligned as transverse ridges and depressions, that terminate abruptly at steep fronts up to 480 m from the foot of the backing talus (Figs. 2a and 2c). Smaller slope-foot boulder accumulations in the same area take the form of linear or arcuate ridges or benches extending up to 45 m from the talus foot, and also terminating abruptly on the adjacent level ground (Fig. 2b). He initially interpreted the larger boulder accumulations as talus rock glaciers and the smaller features as protalus ramparts, but later reinterpreted them as probable RSF runout debris accumulations (Wilson, 2004b). Recent reappraisal of putative Lateglacial ‘rock glaciers’ in the British mountains has similarly concluded that all or almost all of these did not involve deformation of buried ice or ice-rich sediment, the defining criterion of rock glaciers (Ballantyne *et al.,* 2009; Jarman *et al.,* 2013). Re-interpretation of the Errigal-Muckish debris accumulations as RSF runout deposits implies that they represent some of the largest catastrophic RSFs hitherto documented in the British Isles, collectively involving ~41.3 Mt of debris, with individual RSFs exceeding 5 Mt (Table 1). The outlying Slieve League RSF extended to the crest of the southern ridge of the mountain and deposited a broad lobe of large boulders that terminates abruptly on the adjacent valley floor (Fig. 2d).

The dimensions and characteristics of the nine sampled RSFs have been described in detail by Wilson (1990a, 1990b, 1993, 2004b) and are summarised in Table 1. In all cases the failure plane extends to, or very near to, the crest of the slope and is defined by a cliffed headscarp (Fig. 1), with extensive talus accumulations occupying mid- to lower slopes above the RSF runout deposits. Although the quartzite bedding of the Errigal-Muckish chain is steeply dipping (30–60°), none of the sampled RSFs in this area is aligned along the direction of dip (Table 1), implying that failure occurred as an avalanche of fractured rock rather than sliding along a bedding plane. Only the Slieve League RSF failure plane is aligned along the dip of the rock, and in this case failure may have taken place as a translational rockslide. None of the sampled RSF sites exhibits evidence of modification or transport of RSF debris by glacier ice, implying that all RSFs occurred after ice-sheet deglaciation.

Sampling and sample analysis

Twenty-seven samples (three from each of the nine RSF runout deposits) were chiseled from the upper surfaces of large (usually >1 m^3) quartzite boulders (Fig. 3a-c). All samples were collected from distal areas of the debris accumulations except at the Aghla More (West) RSF, where extensive peat and vegetation cover forced us to sample ~25-30 m from the foot of the failed slope. Three additional samples were collected from the lee side of glacially-plucked bedrock on the col that separates Errigal from Mackoght to provide an age for the final deglaciation of the Errigal-Muckish mountains (Fig. 3d). A compass and clinometer were used to record the geometry of the sampled surfaces and the surrounding skyline topography. Locations and altitudes were determined with a hand-held GPS unit, cross-referenced to a 1:50,000 topographic map. Site and sample details are given in Table 2.

All samples were prepared for ^{10}Be analysis at the NERC Cosmogenic Isotope Analysis Facility at SUERC, East Kilbride. Quartz was separated from the 250–500 µm fraction using magnetic and chemical techniques. The isolated quartz was pre-cleaned in a mixture (2:1 by volume) of ~31% (wt/wt) hexafluorosilicic acid and 32% (wt/wt) hydrochloric acid on a shaker table to remove remaining contaminants without dissolving quartz. The final purification of the samples was carried out with 2% (wt/wt) hydrofluoric acid. The procedure is modified from Kohl and Nishiizumi (1992). BeO targets were prepared for $^{10}Be/^{9}Be$ analysis using procedures described in Wilson *et* *al.* (2008) as modified in Glasser *et al.* (2009), and $^{10}Be/^{9}Be$ ratios were measured with the 5 MV Pelletron AMS at SUERC (Xu *et al.,* 2010). $^{10}Be/^{9}Be$ ratios were normalized to NIST SRM 4325 with a $^{10}Be/^{9}Be$ ratio of 2.79×10^{-11} (in agreement with Nishiizumi *et al*., 2007). The standard uncertainties of the cosmogenic nuclide concentrations include 2.5% for the uncertainty related to chemical preparation.

Calibration and scaling of exposure ages

Exposure ages were calculated using the CRONUS-Earth online calculator (Balco *et al*., 2008) and calibrated using two locally-derived ^{10}Be production rates. Local production rates (LPRs) were employed because scaling uncertainty is minimised (e.g. Balco *et al*., 2009; Kaplan *et al*., 2010; Balco, 2011), so the precision of derived exposure ages is significantly improved. The first LPR we employ, the Loch Lomond LPR (LL LPR), is based on ^{10}Be concentration in samples from boulders on an independently-dated YDS terminal moraine in central Scotland, ~260 km ENE of our sampling sites and yields a reference ^{10}Be production rate (Lm scaling) of 3.92 ± 0.18 atoms g^{-1} a^{-1} (Fabel *et al*., 2012; D. Fabel, personal communication, November 2012). The second is the NWH11.6 LPR, which is based on ^{10}Be concentration in samples from bedrock surfaces and glacially-deposited boulders inside the limits of small YDS glaciers in NW Scotland, ~400 km NNE of our sampling sites. The NWH11.6 LPR is based on an assigned deglacial exposure age of 11.6 ± 0.3 ka, yielding a reference ^{10}Be production rate (Lm scaling) of 4.20 ± 0.14 atoms g^{-1} a^{-1}. These two LPRs were selected as they yield the oldest (LL LPR) and youngest (NWH11.6 LPR) exposure ages for our samples (cf. Fabel *et al*., 2012), thus effectively bracketing the range of possible ages. For our samples, use of the NWH11.6 LPR produces exposure ages 6.88–7.01% lower than use of the LL LPR, or roughly 1000 years younger for LL LPR ages of 14–15 ka.

Here we report ages scaled using the time-dependent Lm scheme (Lal, 1991; Stone, 2000), which is widely used in studies of deglaciation chronology in the British Isles. Other scaling schemes (Balco *et al.,* 2008) produce ages up to 1.5% greater or up to 0.5% less than the Lm scheme. We assume a surface erosion rate (ε) of 1 mm ka^{-1} for our samples, which is reasonable for crystalline rocks (Ballantyne, 2010). Assumption of $\varepsilon = 0$ reduces our reported ages by ~1%, and assumption of $\varepsilon = 2$ mm ka^{-1} increases the reported ages by a similar margin. Use of a particular scaling scheme or erosion rate has negligible effect on the temporal pattern of RSFs relative to deglaciation age, as all ages are affected proportionally. Uncertainties cited in the text are external (total) uncertainties at ± 1σ.

Data Filtering

The exposure ages calculated for all 30 samples in our survey are summarised in Table 3 and Fig. 4. To establish best-estimate ages for the timing of failure at each site, we filtered the age data using two independent protocols. We first employed the two-sample difference of means test (using internal uncertainties, as production-rate and scaling uncertainties do not differ at a single site) at $p < 0.05$ to identify statistically-different outlier ages. We then used the reduced chi-square test to establish that the remaining ages for individual sites are consistent with sampling from a single normally-distributed age population. Although all but one of our sample sites yielded pairs or triplets of consistent ^{10}Be exposure ages, six samples (asterisked in Table 3 and Fig. 4) yielded ages significantly different ($p < 0.05$) from those of other samples from the same site. Positive anomalies we attribute to sampling surfaces that were located at or near the ground surface prior to failure, and thus exposed to cosmic radiation before the RSF occurred (Ivy-Ochs *et al*., 2009; Ivy-Ochs and Schaller, 2010). Negative anomalies probably reflect shielding by former sediment cover (Putkonen and Swanson, 2003; Heyman *et al*., 2011) or sampling a boulder emplaced by rockfall subsequent to the main RSF event. When these apparently anomalous ages are excluded, reduced χ^2 values for all but two sites fall below unity, consistent with pairs or triplets of ages belonging to the same age population (Balco, 2011).

The three samples from the Aghla Beg RSF site produced a reduced χ^2 value exceeding unity (1.25), but as no sample age from this site differs from any other at $p < 0.05$ we use all three ages to grenerate the best-estimate age of failure. The Errigal 1 site is problematic, as all three exposure ages differ at $p < 0.05$. For this site we based RSF age on the two closest ages (samples ERGL-1-03 and ERGL-1-04), but note that the derived best-estimate age for this site is less closely constrained than for all other sites where consistent ages were obtained for two or three independent samples. Uncertainty-weighted mean ages (weighted over the inverse squares of the absolute internal uncertainties) were calculated for all sites based on the pairs or triplets of consistent ages, excluding the six anomalous ages asterisked in Table 2 and

Fig.4, and are assumed to represent the best estimate of the timing of deglaciation (Errigal col site) or rock slope failure.

Results

In the discussion below we cite the weighted mean ages derived using LL LPR first, followed by the equivalent ages calculated using NWH11.6 LPR in brackets. Calculation of the significance of differences in age between sites was carried out using the two-sample difference of means test.

Deglaciation age

The deglaciation ages for the Errigal col range from 17.0 ± 1.0 ka (15.9 ± 0.8 ka) to 17.6 ± 1.0 ka (16.5 ± 0.8 ka). In view of the tight clustering of these ages, the derived weighted mean age of 17.4 ± 0.9 ka (16.3 ± 0.7 ka) is accepted as representative for the final disappearance of glacier ice from the Errigal-Muckish mountains, and the temporal datum against which the timing of the eight Errigal-Muckish RSFs can be assessed. The recalibrated age of 19.3 ± 1.0 ka (18.1 ± 0.8 ka) obtained for a bedrock sample by Ballantyne *et al.* (2007) from a site 8.5 km NW of the Slieve League RSF is assumed to approximate the deglaciation age of the latter.

RSF Ages

The weighted mean ages of the nine RSFs range from 17.7 ± 0.9 ka (16.6 ± 0.7 ka) to 12.5 ± 0.7 ka (11.7 ± 0.5 ka). Thus, irrespective of the assumed LPR, all sampled RSFs appear to have occurred during the Late Devensian (Late Weichselian) Lateglacial, in the interval between ice-sheet deglaciation and the beginning of the Holocene. The weighted mean ages for two RSFs, Errigal 4 (17.7 ± 0.9 ka (16.6 ± 0.7 ka)) and Aghla More East (17.2 ± 0.9 ka (16.1 ± 0.7 ka)) are statistically indistinguishable from the assumed deglaciation age of 17.4 ± 0.9 ka (16.3 ± 0.7 ka) of the Errigal col, suggesting that failure at these sites occurred during or within a few centuries following deglaciation. All other sites are significantly younger ($p < 0.05$) than the assumed deglaciation age and failed roughly 1300–4900 years after deglaciation. If the two youngest RSFs (Mackoght: 12.5 ± 0.7 ka (11.7 ± 0.5 ka) and Aghla More West: 13.0 ± 0.7 ka (12.2 ± 0.5 ka)) are excluded, all RSFs occurred within ~2000 years following deglaciation.

Collectively, the nine RSF ages imply that the frequency of failure peaked 1400–1500 years after deglaciation (Fig. 5). In terms of the hypotheses outlined in the introduction, our results show that most of the dated Donegal RSFs do not represent rapid and immediate response to deglaciation, but that RSF activity occurred over a few millennia during the Lateglacial period, broadly in accordance with several previous studies (Blikra *et al.,* 2006; Prager *et al.,* 2008; Fauqué *et al.,* 2009; Longva *et al.,* 2009). There is nonetheless some correspondence with the 'rapid plus delayed' response model proposed by Ballantyne and Stone (2013) for RSFs in the Scottish Highlands, as two RSFs (Errigal-4 and Aghla More East) appeared to have failed during or very shortly after deglaciation, and two more (Mackoght and Aghla More West) over 4000 years after deglaciation. Our results, however, conclusively refute extension of failure throughout the postglacial period without significant clustering.

Discussion: implications of RSF timing for failure mechanisms

In situations where RSFs are known to have occurred during or soon after local deglaciation, explanations for such failures have focused on three possibilities: (1) 'debuttressing' (removal of supporting glacier ice) and paraglacial stress release; (2) palaeoseismicity, and particularly earthquakes triggered by differential glacio-isostatic crustal uplift; and (3) climatic factors, notably enhanced cleft-water pressures or warming and thaw of ice-bonded rock. Such explanations are not mutually exclusive, and may operate in some combination to first weaken rock masses then precipitate kinematic release.

'Debuttressing' and paraglacial stress release

The role of 'debuttressing' or removal of supporting glacier ice as a factor in triggering RSFs has been invoked by several authors (e.g. Agliardi *et al.,* 2009; Ivy-Ochs *et al.* 2009; Hippolyte *et al.,* 2012), but has been challenged on the grounds that glacier ice is liable to deform under pressures imposed by an unstable rock mass (McColl *et al.,* 2010; McColl, 2012; McColl and Davies, 2013). As all but two of our dated RSFs are significantly younger than the timing of local deglaciation (by > 1300 years), this mechanism can be ruled out as a general explanation for the timing of paraglacial RSFs in Donegal.

Conversely, paraglacial (glacially-conditioned) stress release has been widely cited as a causal factor in the failure of rock slopes in formerly glaciated mountain areas, though the process is incompletely understood. Some authors have emphasized the role of differential loading by glacier ice and subsequent unloading during deglaciation in altering the state of stress within rockwalls (e.g. Wyrwoll, 1977; Augustinus, 1995; Ballantyne, 2002; Cossart *et al.,* 2008; Mercier *et al.,* 2013). Others have focused on the effects of glacial erosion in changing the stress field within rock slopes, or the role of glacier ice in suppressing *in situ* stresses resulting from the tectonic and erosional history of the rock mass, with consequent reduction of confining stresses during deglaciation (Leith *et al.,* 2010, 2011; McColl, 2012). Irrespective of the cause of stress release, it is widely accepted that it is responsible for fracture propagation within deglaciated rock slopes, and particularly the development of slope-parallel sheeting joints that constitute potential failure planes (McColl, 2012). Stress release and associated fracturing represent the time-dependent release of elastic strain energy in the unloaded rock, and may potentially reduce rock slopes to a state of critical stability whereby failure may be induced either through progressive loss of intrinsic rock mass strength (Kemeny, 2003; Eberhardt *et al.,* 2004; Brideau *et al.,* 2009), or by transient loss of strength due to an extrinsic trigger. Geotechnical modeling by Gugliemi and Cappa (2010) indicates that the progressive loss of rock mass strength initiated by paraglacial stress release may extend over several millennia, suggesting that the Donegal RSFs may have occurred without any extrinsic trigger. If so, progressive relaxation of rock mass strength to a critical level occurred over a timescale of roughly 0–5000 years, reaching a peak approximately 1450 years after deglaciation (Fig. 5).

Glacio-isostatic uplift and palaeoseismicity

Moderate to large magnitude earthquakes commonly trigger RSFs in tectonically active mountain belts (Keefer, 1984, 1994; Meunier *et al.,* 2007), prompting several researchers to suggest a link between Lateglacial RSF activity and a period of more active seismicity following deglaciation (e.g. Sissons and Cornish, 1982; Ballantyne, 1997; Morner, 2004; Hippolyte *et al.,* 2006; Lagerbäck and Sundh, 2008; Sanchez *et al.,* 2010). In common with the rest of the British Isles, present-day seismic activity in Donegal is subdued (Blake, 2006), and seismic events with $M_L > 4$ are rare (Musson, 2007). However, there is evidence that earthquake activity in tectonically-stable intraplate locations was much greater following Late Pleistocene glaciation than at present (Gregerson and Basham, 1989; Stewart *et al.,* 2000; Morner, 2005). Such enhanced seismicity has usually been attributed to glacio-isostatic crustal uplift acting in conjunction with elastically stored tectonic stresses, though because of the prolonged response time of the resulting large-scale changes in crustal stress, periods of enhanced post-glacial seismicity may lag deglaciation by centuries or millennia (Muir-Wood, 2000).

Evidence for enhanced Lateglacial seismicity is lacking for NW Ireland, but Knight (1999) has described convincing stratigraphic evidence for metre-scale normal faulting triggered by ice unloading during the final phase of glaciation in the southern Sperrin Mountains, 75 km SE of Errigal. This is consistent with the magnitude of postglacial vertical displacements due to differential crustal rebound in the Scottish Highlands (Firth and Stewart, 2000; Stewart *et al.,* 2001). Evidence of seismically-triggered sediment deformation structures in the same region have been interpreted as the products of $M \approx 4.6–6.4$ earthquakes, but though some structures are demonstrably of Lateglacial or early Holocene age, the dating evidence is of poor resolution (Firth and Stewart, 2000).

Enhanced seismic activity probably coincided with the period of most rapid glacio-isostatic crustal uplift. Although no evidence is available for rates of uplift in NW Ireland, it is notable that around the coasts of Scotland the most rapid uplift invariably occurred prior to ~12.8 ka (Firth and Stewart, 2000, table 1), and was thus broadly coincident with the timing of the dated RSFs in Donegal. Such coincidence between two temporal datasets of poor resolution does not necessarily imply causality, but it does suggest that medium to large magnitude Lateglacial seismic events may have played a key role in triggering failure of rock masses previously weakened by stress release and resulting fracture propagation. Additionally, it is notable that all the dated RSFs appear to reflect kinematic release of rock masses along failure planes that extend to, or near to, the slope crest (Table 1). Densmore and Hovius (2000) have shown that such full-slope failures are characteristic of coseismic RSFs, as topographic amplification of ground acceleration during earthquakes tends to trigger failure at or near slope crests (Geli *et al.,*1988; Murphy, 2006).

Climatically-induced RSF triggers

Three climatically-driven factors have been suggested by McColl (2012) as possible triggers of paraglacial RSFs: (1) permafrost degradation, leading to warming and thaw of joint ice that bonds the rock mass (e.g. Davies *et al.,* 2001; Gruber and Haeberli, 2007; Krautblatter *et al.,* 2012, 2013); (2) enhanced cleft-water pressures; and (3) freeze-thaw activity. However, as annual freeze-thaw cycles affect only the outermost few metres of rock slopes (Matsuoka, 1994; Matsuoka *et al.,* 1998), they play an important role in triggering rockfall (e.g. Gruber *et al.,* 2004; Matsuoka and Murton, 2008; Ravanel and Deline, 2011) and may contribute to fracture extension, but are unlikely to trigger deep-seated RSFs.

Figure 6 depicts the timing of the dated RSFs plotted against proxy temperature data for the period 19–11 ka. Permafrost aggradation is known to have occurred in areas exposed by ice-sheet retreat and downwastage within the interval ~19–14.7 ka, and in unglacierised areas during the YDS of ~12.9–11.7 ka (Ballantyne and Harris, 1994; Huijzer and Vandenberghe, 1998). Under stadial conditions, permafrost degradation and consequent warming and thaw of ice-bonded rockwalls is unlikely. Conversely, extensive permafrost degradation is likely to have accompanied and followed rapid warming during stadial to interstadial transitions at ~14.7 ka and ~11.7 ka (Fig. 6). In Donegal, organic sedimentation dated to ~15.3 cal ^{14}C ka in Lough Nadourcon, 7 km SE of Muckish, provides evidence of warming at the end of the Dimlington Stade (Watson *et al.,* 2010).

All nine RSF ages calibrated using LL LPR pre-date the rapid warming events at ~14.7 ka and ~11.7 ka (Fig. 6), implying that warming and thaw of permafrost ice in ice-bonded rock was not a factor in kinematic release of fractured rock masses. Seven RSF ages calibrated using NWH11.6 LPR also pre-date these two warming events, but those of the Ardloughnabrackbaddy and Aghla Beg RSFs (14.5 ± 0.6 ka and 14.5 ± 0.7 ka respectively) closely post-date rapid warming at ~14.7 ka. Four other RSF ages pre-date stadial to interstadial warming events but overlap the timing of these events at -1σ. Collectively, the timing of the RSFs in our sample suggests that warming and thaw of ice-bonded rock was not implicated in catastrophic failure in all or the majority of the RSFs in our sample, but may have precipitated failure in a few cases.

Similarly, development of excess cleft-water pressures would have been impossible under stadial conditions, as liquid water could not have penetrated below the depth of the former active layer without freezing. Irrespective of the calibration employed, almost all RSF ages fall within the Dimlington Stade or Younger Dryas Stade (Fig. 6), implying that that cleft-water pressure build up could have triggered failure in only a few cases.

Wider implications

The weighted mean ages of the nine Lateglacial RSFs in Donegal (17.7 ± 0.9 ka (16.6 ± 0.7 ka) to 12.5 ± 0.7 ka (11.7 ± 0.5 ka)) are remarkably consistent with those of other RSFs in the British Isles at sites that escaped glacier reoccupance during the YDS of ~12.9–11.7 ka. Ballantyne *et al.* (2013) have shown that at least three and probably all of five of the quartzite RSFs that they dated on the Isle of Jura (160 km NE of Errigal) occurred between 15.4 ± 0.9 ka and 12.8 ± 0.6 ka; earlier RSFs are lacking on Jura as it was deglaciated later (~16.8–15.8 ka) than Donegal. Similarly, five RSF runout deposits from granite or sandstone RSFs outside the Younger Dryas glacier limits in the Scottish Highlands yielded ages ranging from ~16.9 ka to ~12.8 ka (Ballantyne and Stone, 2013). In total, for areas deglaciated during the retreat of the last ice sheet and not subsequently reoccupied by glacier ice, only one RSF out of 20 dated sites definitely occurred after ~11.7 ka: a rockslide in lavas that occurred on the Isle of Skye at ~6.1 ka (Ballantyne *et al.,* 1998). It follows that the great majority of undated RSFs in areas occupied by the last British-Irish Ice Sheet but outside the limits of Younger Dryas glaciation are also of Lateglacial (> 11.7 ka) age.

Following complete or near-complete deglaciation of the British Isles during the Lateglacial Interstade (~14.7–12.9 ka; Figure 6), glacier ice expanded during the YDS across much of the Western Highlands of Scotland, with peripheral icefields and numerous smaller glaciers reoccupying mountain areas in Scotland, Wales, Ireland and the English Lake District (Golledge, 2010). A further implication of the temporal concentration of Lateglacial RSF activity prior to ~11.7 ka described above is that numerous catastrophic Lateglacial RSFs presumably also occurred *inside* the Younger Dryas glacial limits during the interval between ice-sheet deglaciation and the end of the YDS at ~11.7 ka, both prior to Younger Dryas glacier expansion and on unglacierised slopes above glaciers during the YDS. Because the debris from such RSFs has been removed by glacier ice, however, these RSF are represented only by failure scars comprising a steep headwall and subjacent failure plane, and lack runout deposits. Dating and systematic mapping of such failure scars remains to be carried out, but it seems likely that glacially-modified Lateglacial RSFs played an important role in trough widening, cirque evolution and the sediment budget of Younger Dryas glaciers (Ballantyne, 2013). In particular, Lateglacial RSFs probably furnished much of the debris at sites where massive end moraines mark the limits of small cirque glaciers, and possibly made a major contribution of sediment to hummocky recessional moraines of YDS age.

More generally, our findings contribute to a growing body of evidence that paraglacial RSF activity following ice-sheet retreat in tectonically-stable intraplate terrains was focused within a few millennia during and following deglaciation (Morner, 2004; Blikra *et al.,* 2006; Longva *et al.,* 2009; Ballantyne and Stone, 2013; Mercier *et al.,* 2013; Ballantyne *et al.,* 2013). This pattern may simply reflect the effects of time-dependent release of elastic strain energy and consequent stress release in promoting fracture propagation and progressive reduction in rock mass strength until failure occurred spontaneously. The broad coincidence in timing between Lateglacial RSFs and the period of rapid glacio-isostatic crustal uplift, however, suggests that moderate to large magnitude earthquakes may also have played an important role in triggering the failure of fractured rock masses. In the case of the nine dated Donegal RSFs, glacial ‘debuttressing’, permafrost degradation or enhanced cleft-water pressures can be excluded as triggers of failure in all but a few cases.

Conclusions

1. Surface exposure dating using cosmogenic ^{10}Be implies that ice-sheet deglaciation of mountain areas of Donegal occurred at ~17.4 ka (LL LPR) to ~16.3 ka (NWH11.6 LPR), depending on the ^{10}Be production rate (LPR) assumed in the age calculation. ^{10}Be exposure dating of the runout debris from nine quartzite RSFs in the same area produced weighted mean ages of 17.7 ± 0.9 ka to 12.5 ± 0.7 ka (LL LPR) or 16.6 ± 0.7 ka to 11.7 ± 0.5 ka (NWH11.6 LPR). Irrespective of assumed ^{10}Be production rate, these ages imply that all nine RSFs occurred within ~5000 years following deglaciation, and that all but two occurred within ~2000 years after deglaciation, with a peak of RSF activity 1400–1500 years after ice-sheet retreat.

2. As all but two of the dated RSFs significantly post-date deglaciation, glacial 'debuttressing' can be excluded as a cause of failure in seven cases. Stress release due to deglacial unloading and/or reduction in confining stress is inferred to have contributed to rock mass weakening through progressive fracture extension, and could have caused intrinsic failure of some or all of the dated RSFs without extrinsic perturbation.

3. Most RSFs occurred under stadial conditions prior to rapid warming events at ~14.7 ka and ~11.7 ka. We infer that neither permafrost degradation (warming and thaw of ice-bonded rock) nor enhanced cleft-water pressures (precluded by permafrost) were responsible for triggering failure in the majority of cases.

4. The timing of the nine RSFs coincides broadly with the period of most rapid glacio-isostatic uplift in Scotland. Evidence for approximately coeval faulting and seismic activity suggests that some or all of the dated RSFs may have been triggered by earthquakes acting on fractured rock slopes.

5. The Lateglacial age of the nine RSFs accords with the findings of RSF dating studies elsewhere in the British Isles. Collectively, almost all of 20 dated RSFs located outside the limits of Younger Dryas glaciation occurred in the interval between ice-sheet deglaciation and ~11.7 ka. One implication is that the great majority of undated RSFs in mountain areas of the British Isles outside the Younger Dryas ice limits are also probably of Lateglacial age. Another is that numerous Lateglacial RSFs also occurred within mountain areas that were reoccupied by glacier ice during the YDS, but that the runout debris from these RSFs has been removed by glacial erosion.

Our results provide strong support for the view that paraglacial RSF activity following ice-sheet retreat in tectonically stable intraplate terrains was concentrated within a few millennia following ice-sheet deglaciation. The generality of this conclusion, however, requires testing on other lithologies. Priorities for further research include dating of postglacial fault scarps to investigate more closely the temporal connection between palaeoseismicity and Lateglacial RSFs (cf. Sanchez *et al.,* 2010), and establishing the ages of deep-seated gravitational slope deformations, which constitute many of the largest RSFs in the British Isles (Jarman, 2006) but have not hitherto been dated.

Acknowledgements

This research was supported by the NERC Cosmogenic Isotope Analysis Facility through award of sample preparation and analysis (CIAF project 9046.0308). We thank Dr Derek Fabel of the University of Glasgow and Professor John Stone of the University of Washington for permission to use ^{10}Be calibration datasets in advance of publication. We also thank Graeme Sandeman for drafting the figures. Sam Smyth, Dave Southall and Bernie Lafferty assisted with sample collection.

Abbreviations. RSF, rock slope failure; YDS, Younger Dryas Stade; LL LPR, Loch Lomond local production rate; NWH11.6 LPR, Northwest Highlands (11.6 ka) local production rate.

References

Abele G. 1974. Bergstürze in den Alpen: Ihre Verbreitung, Morphologie und Folgeerscheinungen. *Deutscher und Österreichischer Alpenverein, Munich.*

Agliardi F, Crosta GB, Zanchi A, Ravazzi C, 2009. Onset and timing of deep-seated gravitational slope deformations in the eastern Alps, Italy. *Geomorphology* **103**: 113–129.

Allen S, Cox S, Owens I. 2010. Rock avalanches and other landslides in the central Southern Alps of New Zealand: a regional study considering possible climate change impacts. *Landslides* **8**: 33–48.

Antinao JL, Gosse J. 2009. Large rockslides in the southern central Andes of Chile (32-34.5°S): tectonic control and significance for Quaternary landscape evolution. *Geomorphology* **104**: 117–133.

Arsenault AM, Meigs AJ. 2005. Contribution of deep-seated bedrock landslides to erosion of a glaciated basin in southern Alaska. *Earth Surface Processes and Landforms* **30**:1111–1125.

Augustinus PC. 1995. Glacial valley cross-profile development: the influence of in situ rock stress and rock mass strength, with examples from the Southern Alps, New Zealand. *Geomorphology* **14**: 87-97.

Balco G. 2011. Contributions and unrealized potential contributions of cosmogenic-nuclide exposure dating to glacier chronology, 1990-2010. *Quaternary Science Reviews* **30**: 3–27.

Balco G, Stone JO, Lifton NA, Dunai TJ. 2008. A complete and easily accessible means of calculating surface exposure ages or erosion rates from ^{10}Be and ^{26}Al measurements. *Quaternary Geochronology* **3**: 174-195.

Balco G, Briner J, Finkel RC, Rayburn JA, Ridge JC, Schaefer JM. 2009. Regional beryllium-10 production rate calibration for late-glacial northeastern North America. *Quaternary Geochronology* **4**: 93–107.

Ballantyne CK. 1997. Holocene rock-slope failures in the Scottish Highlands. *Paläoklimaforschung* **19**: 197–206.

Ballantyne CK. 2002. Paraglacial geomorphology. *Quaternary Science Reviews* **21**: 1935-2017.

Ballantyne CK. 2010. Extent and deglacial chronology of the last British-Irish Ice Sheet: implications of exposure dating using cosmogenic isotopes. *Journal of Quaternary Science* **25**: 515–534.

Ballantyne CK. 2013. Lateglacial rock-slope failures in the Scottish Highlands. *Scottish Geographical Journal* **129**: 67-84.

Ballantyne CK, Harris C. 1994. *The Periglaciation of Great Britain.* Cambridge University Press: Cambridge.

Ballantyne CK, Stone JO. 2004. The Beinn Alligin rock avalanche, NW Scotland: cosmogenic ^{10}Be dating, interpretation and significance. *The Holocene* **14**: 448-453.

Ballantyne CK, Stone JO. 2009. Rock-slope failure at Baosbheinn Wester Ross, NW Scotland: age and interpretation. *Scottish Journal of Geology* **45**: 177-181.

Ballantyne CK, Stone JO. 2012. Did large ice caps persist on low ground in north-west Scotland during the Lateglacial Interstade? *Journal of Quaternary Science* **27**: 297-306.

Ballantyne CK, Stone JO. 2013. Timing and periodicity of paraglacial rock-slope failures in the Scottish Highlands. *Geomorphology* **186**: 150-161.

Ballantyne CK, McCarroll D, Stone JO. 2007. The Donegal ice dome, northwest Ireland: dimensions and chronology. *Journal of Quaternary Science* **22**: 773-783.

Ballantyne CK, Schnabel C, Xu S. 2009. Exposure dating and reinterpretation of coarse debris accumulations ('rock glaciers') in the Cairngorm Mountains, Scotland. *Journal of Quaternary Science* **24**: 19-31.

Ballantyne CK, Wilson P, Gheorghiu D, Rodés A. 2013. Timing and causes of rock-slope failure, Isle of Jura, Scotland. *Earth Surface Processes and Landforms* (in press).

Ballantyne CK, Stone JO, Fifield LK. 1998. Cosmogenic Cl-36 dating of postglacial landsliding at The Storr, Isle of Skye, Scotland. *The Holocene* **8**: 347-351.

Bigot-Cormier F, Braucher R, Bourlès D, Guglielmi Y, Dubar M, Stéphan J-F. 2005. Chronological constraints on processes leading to large landslides. *Earth and Planetary Science Letters* **235**: 141–150.

Blake T. 2006. Measuring Ireland's earthquakes. *Extractive Industry Ireland* **2006**: 78-81.

Blikra LH, Longva O, Braathen A, Anda E, Dehls JF, Stalsberg K. 2006. Rock slope failures in Norwegian fjord areas: examples, spatial distribution and temporal pattern. In: Evans SG, Mugnozza GS, Strom A, Hermanns RL, (eds). *Landslides from massive rock slope failure*. Springer, Dordrecht, 475-496.

Brideau M-A, Yan M, Stead D. 2009. The role of tectonic damage and brittle rock failure in the development of large rock failures.*Geomorphology* **103**: 30–49.

Brooks SJ, Birks HJB. 2000. Chironomid-inferred Late-glacial air temperatures at Whitrig Bog, southeast Scotland. *Journal of Quaternary Science* **15**: 759–764.

Charlesworth JK. 1924. The glacial geology of the north-west of Ireland. *Proceedings of the Royal Irish Academy* **B36**: 174-314.

Clark J, McCabe AM, Schnabel C, Clark PU, Freeman S, Maden C, Xu S. 2009. ^{10}Be chronology of the last deglaciation of County Donegal, northwestern Ireland. *Boreas* **38**: 111-118.

Cossart E, Braucher R, Fort M, Bourlès DL, Carcaillet J. 2008. Slope instability in relation to glacial debuttressing in alpine areas (Upper Durance catchment, southeastern France): Evidence from field data and ^{10}Be cosmic ray exposure ages. *Geomorphology* **95**: 3-26.

Cruden DM, Hu XQ. 1993. Exhaustion and steady state models for predicting landslide hazards in the Canadian Rocky Mountains. *Geomorphology* **8**: 279-285.

Davies MCR, Hamza O, Harris C. 2001. The effect of rise in mean annual temperature on the stability of rock slopes containing ice-filled discontinuities. *Permafrost and Periglacial Processes* **12**: 137–144.

Densmore AL, Hovius N. 2000. Topographic fingerprints of bedrock landslides. *Geology* **28**: 371–374.

Dortch JM, Owen LA, Haneberg WC, Caffee MW, Dietsch C, Kamp U, 2009. Nature and timing of large landslides in the Himalaya and Transhimalaya of northern India. *Quaternary Science Reviews* **28**: 1037–1054.

Eberhardt E, Stead D, Coggan JS. 2004. Numerical analysis of initiation and progressive failure in natural rock slopes – the 1991 Randa rockslide. *International Journal of Rock Mechanics and Mining Science* **41**: 69–87.

Evans SG, Clague JJ. 1994. Recent climate change and catastrophic geomorphic processes in mountain environments. *Geomorphology* **10**: 107–128.

Fabel D, Ballantyne CK, Xu S. 2012. Trimlines, blockfields, mountain-top erratics and the vertical dimensions of the last British-Irish Ice Sheet in NW Scotland. *Quaternary Science Reviews* **55**: 91-102.

Fauqué L, Hermanns RL, Hewitt K, Rosas M, Wilson C, Baumann V, Lagorio S, Di Tommaso I. 2009. Mega-deslizamientos de la pared sur del Cerro Aconcagua y su relación con depósitos asignados a la glaciación Pleistocena. *Revista de la Asociación Geológica Argentina* **65**: 691–712.

Firth CR, Stewart IS. 2000. Postglacial tectonics of the Scottish glacio-isostatic uplift centre. *Quaternary Science Reviews* **19**: 1469–1493.

Geli L, Bard P-Y, Jullien B. 1988. The effect of topography on earthquake rebound motion: a review and new results. *Seismological Society of America Bulletin* **78**: 42–63.

Glasser NF, Clemmens S, Schnabel C, Fenton CR, McHargue L. 2009. Tropical glacier advances in the Cordillera Blanca, Peru between 12.5 and 7.6 ka from cosmogenic ^{10}Be dating. *Quaternary Science Reviews* **28**: 3448–3458.

Golledge NR. 2010. Glaciation of Scotland during the Younger Dryas Stadial: a review. *Journal of Quaternary Science* **25**: 550–566.

Gregerson S, Basham PW. (eds.) 1989.*Earthquakes at North Atlantic passive margins: neotectonics and postglacial rebound.* Kluewer: Dordrecht.

Gruber S, Hoezle M, Haeberli W. 2004. Permafrost thaw and destabilization of Alpine rock walls in the hot summer of 2003. *Geophysical Research Letters* **31**: L13504.

Gruber S, Haeberli W. 2007. Permafrost in steep bedrock slopes and its temperature-related destabilization following climate change. *Journal of Geophysical Research* **112**: F02S18.

Gugliemi Y, Cappa F. 2010. Regional-scale relief evolution and large landslides: insights from geomechanical analyses in the Tinée Valley (southern French Alps). *Geomorphology* **117**: 121–129.

Haeberli W, Wegmann M, VonderMühll D. 2008. Slope stability problems related to glacier shrinkage and permafrost degradation in the Alps. *Eclogae Geologicae Helvetiae* **90**: 407–414.

Hermanns RL, Niedermann, S. 2011. Late Pleistocene–early Holocene palaeoseismicity deduced from lake sediment deformation and coeval landsliding in the Calchaquíes valleys, NW Argentina. *Geological Society of America Special Paper* **479**: 181–194.

Hermanns RL, Schellenberger A. 2008. Quaternary tephrochronology helps define conditioning factors and triggering mechanisms of rock avalanches in NW Argentina. *Quaternary International* **178**: 261-275.

Hermanns R, Niedermann S, Ivy-Ochs S, Kubik P. 2004. Rock avalanching into a landslide-dammed lake causing multiple dam failure in Las Conchas valley (NW Argentina) – evidence from surface exposure dating and stratigraphic analyses. *Landslides* **1**: 113-122.

Hewitt K, Clague JJ, Orwin JF. 2008. Legacies of catastrophic rock slope failures in mountain landscapes. *Earth-Science Reviews* **87**: 1-38.

Hewitt K, Gosse J, Clague JJ. 2011. Rock avalanches and the pace of Late Quaternary development of river valleys in the Karakoram Himalaya. *Geological Society of America Bulletin* **123**: 1836–1850.

Heyman J, Stroeven AP, Harbor JM, Caffee MW. 2011. Too young or too old: evaluating cosmogenic exposure dating based on an analysis of compiled boulder exposure ages. *Earth and Planetary Science Letters* **302**: 71–80.

Hippolyte J-C, Bourlès D, Braucher R, Carcaillet J, Léanni L, Arnold M, Aumaître G. 2009. Cosmogenic ^{10}Be dating of a sackung and its faulted rock glaciers, in the Alps of Savoy (France). *Geomorphology* **108**: 312–320.

Hippolyte J-C, Bourlès D, Léanni L, Braucher R, Chauvet F, Lebatard AE. 2012. ^{10}Be ages reveal >12 ka of gravitational movement in a major sackung of the western Alps (France). *Geomorphology* **171–172**: 139–153.

Hormes A, Ivy-Ochs S, Kubik PW, Ferreli L, Michetti AM. 2008. ^{10}Be exposure ages of a rock avalanche and a late glacial moraine in the Alta Valtellina, Italian Alps. *Quaternary International* **190**: 136–145.

Huijzer B, Vandenberghe J. 1998. Climatic reconstruction of the Weichselian Pleniglacial in northwestern and central Europe. *Journal of Quaternary Science* **13**: 391-417.

Ivy-Ochs S, Schaller M. 2010. Examining processes and rates of landscape change with cosmogenic radionuclides. *Radioactivity in the Environment* **16**: 231-294.

Ivy-Ochs S, Poschinger AV, Synal H-A, Maisch M. 2009. Surface exposure dating of the Flims landslide, Graubünden, Switzerland. *Geomorphology* **103**: 104-112.

Jarman D. 2006. Large rock slope failures in the Highlands of Scotland: characterisation, causes and spatial distribution. *Engineering Geology* **83**: 161-182.

Jarman D, Wilson P, Harrison S. 2013. Are there any relict rock glaciers in the British mountains? *Journal of Quaternary Science* **28**: 131–143.

Kaplan MR, Schaefer JM, Denton GH, Barrell DJA, Chinn TJH, Putnam AE, Andersen BG, Finkel RC, Schwartz R, Doughty AM. 2010. Glacier retreat in New Zealand during the Younger Dryas stadial. *Nature* **467**: 194–197.

Keefer DK, 1984. Landslides caused by earthquakes. *Geological Society of America Bulletin* **95**: 406–421.

Keefer DK, 1997. The importance of earthquake-induced landslides to long-term slope erosion and slope-failure hazards in seismically-active regions. *Geomorphology* **10**: 265–284.

Kemeny J. 2003. The time-dependent reduction of sliding cohesion due to rock bridges along discontinuities: a fracture mechanics approach. *Rock Mechanics and Rock Engineering* **36**: 27–38.

Kohl C, Nishiizumi K. 1992. Chemical isolation of quartz for measurement of in situ produced cosmogenic nuclides. *Geochimica et Cosmochimica Acta* **56**: 3586–3587.

Knight J. 1999. Geological evidence for neotectonic activity during deglaciation of the southern Sperrin Mountains, Northern Ireland. *Journal of Quaternary Science* **14**: 45–57.

Korup O, Clague JJ, Hermanns RL, Hewitt K, Strom AL, Weidinger JT. 2007. Giant landslides, topography and erosion. *Earth and Planetary Science Letters* **261**: 578–589.

Krautblatter M, Funk D, Günzel FK. 2013. Why permafrost rocks become unstable: a rock-ice-mechanical model in space and time. *Earth Surface Processes and Landforms* **38**: 876–887.

Krautblatter M, Huggel C, Deline P, Hasler A. 2012. Research perspectives on unstable high-alpine bedrock permafrost: measurement, modelling and process understanding. *Permafrost and Periglacial Processes* **23**: 80–88.

Lal D. 1991. Cosmic ray labeling of erosion surfaces: in situ nuclide production rates and erosion models. *Earth and Planetary Science Letters* **104**: 424–439.

Lagerbäck R, Sundh M. 2008. Early Holocene faulting and palaeoseismicity in northern Sweden. *Geological Survey of Sweden, Research Paper* **C836**: 84 pp.

Leith K, Amann F, Moore JR, Kos A, Loew S. 2010.Conceptual modelling of near-surface extensional fracture in the Matter and Saas Valleys, Switzerland. In:

Geologically Active. Proceedings of the 11th IAEG Congress, Auckland, New Zealand, Williams AL, Pinches GM, Chin CY, McMorran TJ, Massey CI (eds). CRC Press, Boca Raton; 363–371.

Leith K, Moore J, Amann F, Loew S. 2011. Effect of glacial ice cover on fracturing critically stressed bedrock. *Geophysical Research Abstracts* **13**: EGU2011-12825-2.

Long CB, McConnell BJ. 1997. *Geology of north Donegal.* Geological Survey of Ireland, Dublin.

Long CB, McConnell BJ. 1999. *Geology of south Donegal.* Geological Survey of Ireland, Dublin.

Longva O, Blikra LH, Dehls JF. 2009. Rock avalanches: distribution and frequencies in the inner part of Storfjorden, Møre og Romsdal County, Norway. *Geological Survey of Norway Report* **2009.002**: 32 pp.

Lowe JJ, Rasmusson SO, Björk S, Hoek WJ, Steffensen JP, Walker MJC, Yu ZC, INTIMATE Group. 2008. Synchronisation of palaeoenvironmental events in the North Atlantic region during the Last Termination: a revised protocol recommended by the INTIMATE Group. *Quaternary Science Reviews* **27**: 6–17.

Matsuoka N. 1994. Diurnal freeze-thaw depth in rockwalls: field measurements and theoretical considerations. *Earth Surface Processes and Landforms* **19**: 423-455.

Matsuoka N, Hirakawa K, Watanabe T, Haeberli W, Keller F. 1998. The role of diurnal, annual and millennial freeze-thaw cycles in controlling alpine slope stability. In: *Proceedings of the 7th International Conference on Permafrost.* Sainte-Foy; Université Laval, 711–717.

Matsuoka N, Murton J. 2008. Frost weathering: recent advances and future directions. *Permafrost and Periglacial Processes* **19**: 195-210.

McColl ST. 2012. Paraglacial rock-slope stability. *Geomorphology* **153-154**: 1-16.

McColl ST, Davies TRH, 2013. Large ice-contact slope movements: glacial debuttressing, deformation and erosion. *Earth Surface Processes and Landforms* **38**: 1102–1115.

McColl, ST, Davies TRH, McSaveney MJ. 2010. Glacier retreat and rock-slope stability: debunking debuttressing. In: Williams AL, Pinches GM, Chin CY, Massey CI. (eds), *Geologically active*. Taylor & Francis, London, 467-474.

Mercier D, Cossart E, Decaulne A, Feuillet T, Jónsson HP, Sæmundsson Þ. 2013. The Höfðahólar rock avalanche (sturzström): chronological constraint of paraglacial landsliding on an Icelandic hillslope. *The Holocene* **23**: 432-446.

Meunier P, Hovius N, Haines AJ. 2007. Regional patterns of earthquake-triggered landslides and their relation to ground motion. *Geophysical Research Letters* **34**: L20408.

Mitchell WA, McSaveney MJ, Zondervan A, Kim K, Dunning SA, Taylor PJ. 2007. The KeylongSerai rock avalanche, NW Indian Himalaya: geomorphology and palaeoseismic implications. *Landslides* **4**: 245-254.

Morner N-A. 2004. Active faults and palaeoseismicity in Fennoscandia, especially Sweden. Primary structure and secondary effects. *Tectonophysics* **380**: 139–157.

Morner N-A. 2005. An interpretation and catalogue of palaeoseismicity in Sweden. *Tectonophysics* **408**: 265–307.

Muir-Wood R. 2000. Deglaciation seismotectonics: a principal influence on intraplate seismogenesis at high latitudes. *Quaternary Science Reviews* **19**: 1399–1411.

Murphy W. 2006. The role of topographic amplification on the initiation of rock-slope failures during earthquakes. In: Evans SG, Mugnozza GS, Strom A, Hermanns RL, (eds). *Landslides from massive rock slope failure*. Springer, Dordrecht, 139–154.

Musson RMW. 2007. British earthquakes. *Proceedings of the Geologists' Association* **118**: 305-337.

Nishiizumi K, Imamura M, Caffee MW, Southon JR, Finkel RC, McAninch J. 2007. Absolute calibration of ^{10}Be AMS standards. *Nuclear Instruments and Methods in Physics Research B***258**: 403–413.

O'Cofaigh C, Dunlop P, Benetti S. 2012. Marine geophysical evidence for late Pleistocene ice sheet extent and recession off northwest Ireland. *Quaternary Science Reviews* **44**: 147-159.

Penna IM, Hermanns RL, Niedermann S, Folguera A. 2011. Multiple slope failures associated with neotectonic activity in the southern central Andes (37°-37°30´S), Patagonia, Argentina. *Geological Society of America Bulletin* **123**: 1880-1895.

Prager C, Zangerl C, Patzelt G, Brandner R. 2008. Age distribution of fossil landslides in the Tyrol (Austria) and its surrounding areas. *Natural Hazards and Earth Systems Science* **8**: 377-407.

Putkonen J, Swanson T. 2003. Accuracy of cosmogenic ages for moraines. *Quaternary Research* **59**: 255–261.

Rasmussen SO, Andersen KK, Svensson AM, Steffensen JP, Vinther BM, Clausen HB, Siggaard-Andersen ML, Johnsen SJ, Larsen LB, Dahl-Jensen D, Bigler M, Rothlisberger R, Fischer H, Goto-Azuma K, Hansson ME, Ruth U. 2006. A new

Greenland ice core chronology for the last glacial termination. *Journal of Geophysical Research* **111**: D06102.

Ravanel L, Deline P. 2011. Climate influence on rockfalls in high-Alpine steep rockwalls: the north side of the Aiguilles de Chamonix (Mont Blanc massif) since the end of the 'Little Ice Age'. *The Holocene* **21**: 357-365.

Sanchez G, Rolland Y, Corsini M, Braucher R, Bourlès D, Arnold M, Aumaître G. 2010. Relationships between tectonics, slope instability and climate change: cosmic ray exposure dating of active faults, landslides and glacial surfaces in the French Alps. *Geomorphology* **117**: 1–13.

Shroder JF, Owen LA, Seong YB, Bishop MP, Bush A, Caffee MW, Copland L, Finkel RC, Kamp U. 2011. The role of mass movements on landscape evolution in the central Karakoram: discussion and speculation. *Quaternary International* **236**: 34–47.

Sissons JB, Cornish R. 1982. Differential glacio-isostatic uplift of crustal blocks at Glen Roy, Scotland. *Quaternary Research* **18**: 268–288.

Soldati M, Corsini A, Pasuto A. 2004. Landslides and climate change in the Italian Dolomites since the Late glacial. *Catena* **55**: 141–161.

Stewart IS, Firth CR, Rust DJ, Collins PEF, Firth JA. 2001. Postglacial fault movement and palaeoseismicity in western Scotland: a reappraisal of the Kinloch Hourn fault, Kintail. *Journal of Seismology* **6**: 307–328.

Stewart IS, Sauber J, Rose J. 2000. Glacio-seismotectonics: ice sheets, crustal deformation and seismicity. *Quaternary Science Reviews* **19**: 1367–1389.

Stock GM and Uhrhammer RA. 2010. Catastrophic rock avalanche 3600 years BP from El Capitan, Yosemite Valley, California. *Earth Surface Processes and Landforms* **35**: 941-951.

Stone JO. 2000. Air pressure and cosmogenic isotope production. *Journal of Geophysical Research* **105 (B10)**: 23753–23759.

Watson JE, Brooks SJ, Whitehouse NJ, Reimer PJ, Birks HJB, Turney C. 2010. Chironomid-inferred late-glacial summer air temperatures from Lough Nadourcan, Co. Donegal, Ireland. *Journal of Quaternary Science* **25**: 1200-1210.

Wilson P. 1990a. Characteristics and significance of protalus ramparts and fossil rock glaciers on Errigal Mountain, County Donegal. *Proceedings of the Royal Irish Academy* **90B**: 1-21.

Wilson P. 1990b. Morphology, sedimentological characteristics and origin of a fossil rock glacier on Muckish Mountain, northwest Ireland. *Geografiska Annaler* **72A**: 237-247.

Wilson P. 1993. Description and origin of some talus-foot debris accumulations, Aghla Mountains, Co. Donegal, Ireland. *Permafrost and Periglacial Processes* **4**: 231-244.

Wilson, P. 2004a. Evidence for and reconstruction of a Nahanagan Stade glacier at Croloughan Lough, Derryveagh Mountains, Co. Donegal. *Irish Journal of Earth Sciences* **22**: 45-54.

Wilson P. 2004b. Relict rock glaciers, slope failure deposits, or polygenetic features? A re-assessment of some Donegal debris landforms. *Irish Geography* **37**: 77-87.

Wilson P, Bentley M, Schnabel C, Clark R, Xu, S. 2008. Stone run (blockstream) formation in the Falkland Islands over several cold stages, deduced from cosmogenic isotope (^{10}Be and ^{26}Al) dating. *Journal of Quaternary Science* **23**: 461–473.

Wyrwoll K-H. 1977. Causes of rock-slope failure in a cold area: Labrador-Ungava. *Geological Society of America Reviews in Engineering Geology* **3**: 59–67.

Yamasaki S, Chigira M. 2011. Weathering mechanisms and their effects on landsliding in pelitic schists. *Earth Surface Processes and Landforms* **36**: 481–494.

Xu S, Dougans AB, Freeman SPHT, Schnabel C, Wilcken KM. 2010. Improved ^{10}Be and ^{26}Al AMS with a 5 MV spectrometer. *Nuclear Instruments and Methods B***268**: 736-738.

Figure captions

Figure 1. Location of sampled RSFs and the Errigal col sampling site in the Errigal-Muckish mountains. The outlying Slieve League RSF site is not shown.

Figure 2. Donegal RSFs. (a) Hummocky runout debris of the Errigal-4 RSF. Mackoght is the peak to right of centre, with RSF runout debris just above the small lake at the base of the talus. (b) RSF debris lobe at Aghla More East. (c) Muckish RSF showing quarried frontal slope. (d) Slieve League RSF.

Figure 3. (a-c) sampled boulders in RSF runout zones. (a) Sample LA-04. (b) Sample MGHT-02; the survey pole has 20 cm divisions. (c) Sample AB-02. (d) Glacially-plucked quartzite outcrops on the Errigal col, which were sampled to obtain deglaciation age.

Figure 4. Exposure ages obtained for all RSF samples (vertical dashes); horizontal bars represent $\pm 1\sigma$ external uncertainties. Top: ages calculated using LL LPR. Bottom: ages calculated using NWH11.6 LPR. The vertical line represents the uncertainty-weighted mean deglaciation age for the Errigal col, and the shaded area represents the associated $\pm 1\sigma$ external uncertainty. Asterisked (*) ages are anomalous outliers that differ at $p < 0.05$ from other ages obtained at the same site. Note that Slieve League site was deglaciated much earlier, at ~19.1 ka (LL LPR).

Figure 5. Probability density distributions of all RSF ages, calculated as time elapsed since deglaciation (t = 0). Top: calculated using LL LPR. Bottom: calculated using NHW11.6 LPR. Shaded zone represents deglaciation age ($t = 0$) $\pm 1\sigma$ uncertainty. The area under the curve left of t = 0 is a function of the calculation of probability density, which incorporates both weighted means and associated uncertainties. The differing shapes of the two curves reflect the greater uncertainties associated with the LL LPR age calibration (Table 2).

Figure 6. Weighted mean ages (vertical dashes) and associated $\pm 1\sigma$ external uncertainties for the nine dated RSFs plotted against deglaciation age, NGRIP ice core $\delta^{18}O$ data for 12–21 ka (Rasmussen *et al*., 2006), the ice core stages proposed by Lowe *et al*. (2008) and mean July temperature data inferred from chironomid assemblages in SE Scotland (Brooks and Birks, 2000), matched to the NGRIP ice core data. 1: Errigal-4. 2: Aghla More East. 3: Slieve League. 4: Errigal-1. 5: Muckish. 6: Ardloughnabrackbaddy. 7: Aghla Beg. 8: Aghla More West. 9: Mackoght.

Table 1. Characteristics of the sampled RSFs.

Rock-slope failure (Irish Grid Reference)	Bedrock dip direction	RSF aspect	Area[1] (km^2)	Debris mass (Mt)	Crest elevation[2] (m OD)	Toe elevation[3] (m OD)
Errigal 1 (B 918204)	SE	SW	0.55	10	750	150
Errigal 4 (B 935215)	SE	NE	0.6	6.9	750	330
Mackoght (B 937216)	SE	NW	0.06	0.3	550	340
Aghla More West (B 947236)	NW	SW	0.2	0.3	580	150
Aghla More East (B 950242)	NW	NNE	0.09	0.3	580	400
Ardloughnabrackbaddy (B 970250)	NW	NE	0.18	2	600	290
Aghla Beg (B 965257)	NW	NE	0.16	1.7	560	240
Muckish (B 992273)	NW	SW	0.32	7.4	550	200
Slieve League (G 558775)	NE	NE	0.05	ND	500	360

[1] Combined source area and run-out debris. [2] Crest elevation of source area. [3] Lowest e

Characteristics[4]	
Source area	Debris zone
Shattered buttresses and pinnacles with intervening gullies on upper slope, talus sheet with extensive vegetation cover on mid- and lower slopes.	Lobate, multi-ridged accumulation of coarse debris extending 450 m from talus foot. Terminal ridge 36 m thick, 44 m high. Extensive peat and vegetation cover.
Broadly recessed slope 750 m wide; rock buttresses and gullies on upper slope, extensive talus sheet below.	Lobate, mutiple ridges/hummocks of coarse debris extending 480 m from talus foot. Terminal ridge 25 m thick and 25 high.
Planar upper slope of buttresses and gullies, talus sheet below.	Arcuate ridge of debris 36 m from talus foot; 10 m thick, 13 m high.
Recessed slope 250 m wide; shattered buttresses and gullies on upper slope, extensive talus sheet below.	Debris extends downslope in series of steps 10-30 m wide, to 450 m from talus foot. Debris contained within narrow (100-150 m wide) downslope-aligned depression.
Recessed slope 300 m wide; shattered buttresses and gullies on upper slope, extensive talus sheet below.	Debris accumulation is a single ridge in north, multi-ridged feature in south, extending 105 m from talus foot. Terminal ridge 14 m thick, 16 m high.
Recessed slope 250 m wide; little exposed bedrock, talus almost to crest.	Arcuate ridges and hummocks of coarse debris extending 450 m from talus foot, some hummocks up to 32 m in thickness.
Recessed slope 250 m wide; shattered bedrock exposures on upper slope, talus sheet below.	Lobate, multi-ridged accumulation of coarse debris. Terminal ridge 25 m thick and 25 m high.
Planar hillside with prominent buttresses and intervening gullies on upper slope, extensive talus sheet below.	Arcuate ridge of coarse debris at talus foot; basal width >200 m, 55 m thick, 95 m high.
Recessed slope 150 m wide; bedrock cliff across part of upper slope to 10 m high. Headwall crest lowered by 30 m.	Tongue-to-lobate shaped accumulation of coarse debris. Not surveyed in detail

levation of run-out zone. [4] Sources: Wilson (1990a, 1990b, 1993, 2004b).

Table 2. Sample and analytical data

Site and Sample codes	AMS ID	Latitude (°N)	Longitude (°W)	Altitude (m OD)	Thickness (cm)	Density (g cm^{-3})	Shielding correction	^{10}Be (10^3 atoms g^{-1})
Errigal Col								
ERGL-Col-01	b3996	55.03478	8.09863	430	4	2.56	0.9685	9.983 ± 0.357
ERGL-Col-02	b3998	55.03460	8.09859	425	6	2.56	0.9739	10.16 ± 0.328
ERGL-Col-04	b3999	55.03466	8.09843	405	6	2.58	0.8991	9.217 ± 0.319
Errigal-1 RSF								
ERGL-1-01	b3640	55.02900	8.12595	200	3	2.54	0.9897	6.192 ± 0.214
ERGL-1-03	b3628	55.02927	8.12563	200	3	2.59	0.9925	8.373 ± 0.296
ERGL-1-04	b3629	55.02949	8.12676	200	3	2.56	0.9917	7.322 ± 0.274
Errigal-4 RSF								
ERGL-4-01	b3993	55.04000	8.10000	360	4	2.61	0.9862	9.947 ± 0.347
ERGL-4-02	b3994	55.04000	8.10000	358	2.5	2.61	0.9863	9.611 ± 0.345
ERGL-4-03	b3995	55.04000	8.10000	351	2.5	2.61	0.9826	10.20 ± 0.342
Mackoght RSF								
MGHT-01	b3632	55.04073	8.09925	340	3.5	2.65	0.9604	7.779 ± 0.282
MGHT-02	b3633	55.04073	8.09921	340	1.5	2.67	0.9573	6.943 ± 0.246
MGHT-03	b3634	55.04100	8.09861	345	2.5	2.67	0.9565	6.675 ± 0.234
Aghla More (West) RSF								
AMW-01	b3635	55.06034	8.07937	375	3.5	2.61	0.9661	5.299 ± 0.198
AMW-02	b3626	55.06020	8.08081	375	1.5	2.56	0.9620	7.335 ± 0.273
AMW-03	b3636	55.06046	8.08036	375	2.5	2.59	0.9631	7.335 ± 0.238
Aghla More (East) RSF								
AME-01	b3594	55.06546	8.07757	410	6	2.32	0.9715	11.49 ± 0.399
AME-02	b3595	55.06539	8.07755	410	4	2.58	0.9822	10.14 ± 0.354
AME-03	b3596	55.06570	8.07734	405	2.5	2.45	0.9794	9.957 ± 0.347
Ardloughnabrackbaddy RSF								
LA-02	b4137	55.07269	8.04630	335	4	2.56	0.9912	7.545 ± 0.312
LA-03	b4140	55.07261	8.04583	325	6	2.54	0.9906	8.482 ± 0.320
LA-04	b4000	55.07230	8.04479	310	3.5	2.58	0.9896	8.217 ± 0.297
Aghla Beg RSF								
AB-01	b4004	55.07983	8.05682	250	4.5	2.55	0.9875	8.208 ± 0.468
AB-02	b4135	55.08036	8.05672	245	3	2.47	0.9909	7.560 ± 0.312
AB-03	b4136	55.08005	8.05949	252	3.5	2.59	0.9802	7.939 ± 0.357
Muckish RSF								
MK-01	b4001	55.09416	8.00729	315	2	2.48	0.9379	8.179 ± 0.334
MK-03	b4141	55.09435	8.00739	312	1.5	2.46	0.9370	8.455 ± 0.313
MK-05	b4142	55.09395	8.00749	311	2.5	2.52	0.9827	7.770 ± 0.297
Slieve League RSF								
SL-02	b5731	54.64515	8.68262	272	5.2	2.58	0.9766	8.490 ± 0.340
SL-03	b5732	54.64515	8.68262	272	3	2.57	0.9766	9.003 ± 0.442
SL-04	b5733	54.64515	8.68262	272	4.5	2.57	0.9766	8.551 ± 0.423

^{10}Be concentrations are based on 2.79 x 10^{-11} ^{10}Be/Be ratio for NIST SRM4325. Uncertainties (± 1σ) include 1σ uncertainties related to the measurement and measurement repeatability of the sample and the standard material, as well as the blank correction (which is negligible).

Table 3. ^{10}Be exposure ages

Sample	LL LPR			NWH 11.6 LPR		
	Exposure age (ka)	Internal uncertainty (ka)	Total uncertainty (ka)	Exposure age (ka)	Internal uncertainty (ka)	Total uncertainty (ka)
Errigal Col						
ERGL-Col-01	17.03	0.62	1.00	15.93	0.58	0.81
ERGL-Col-02	17.60	0.58	1.00	16.46	0.54	0.79
ERGL-Col-04	17.57	0.62	1.02	16.43	0.58	0.82
Weighted mean	**17.41**	**0.35**	**0.88**	**16.28**	**0.33**	**0.66**
Errigal-1 RSF						
ERGL-1-01*	12.70	0.45	0.73	11.88	0.42	0.59
ERGL-1-03	17.22	0.62	1.01	16.11	0.58	0.81
ERGL-1-04	15.03	0.57	0.90	14.06	0.53	0.73
Weighted mean	**16.04**	**0.42**	**0.86**	**15.00**	**0.39**	**0.66**
Errigal-4 RSF						
ERGL-4-01	17.82	0.64	1.04	16.66	0.59	0.84
ERGL-4-02	17.04	0.62	1.00	15.93	0.58	0.81
ERGL-4-03	18.28	0.63	1.05	17.09	0.59	0.84
Weighted mean	**17.71**	**0.36**	**0.89**	**16.56**	**0.34**	**0.68**
Mackoght RSF						
MGHT-01*	14.47	0.53	0.85	13.53	0.50	0.69
MGHT-02	12.73	0.46	0.74	11.91	0.43	0.60
MGHT-03	12.29	0.44	0.71	11.49	0.41	0.57
Weighted mean	**12.50**	**0.32**	**0.66**	**11.69**	**0.30**	**0.51**
Aghla More West RSF						
AMW-01*	9.43	0.36	0.56	8.82	0.33	0.45
AMW-02	12.95	0.49	0.77	12.11	0.46	0.62
AMW-03	13.04	0.43	0.74	12.19	0.40	0.59
Weighted mean	**13.00**	**0.32**	**0.68**	**12.16**	**0.30**	**0.52**
Aghla More East RSF						
AME-01*	20.15	0.72	1.18	18.84	0.67	0.94
AME-02	17.39	0.62	1.01	16.26	0.58	0.81
AME-03	16.97	0.60	0.99	15.87	0.56	0.79
Weighted mean	**17.18**	**0.43**	**0.90**	**16.06**	**0.40**	**0.69**
Ardloughnabrackbaddy RSF						
LA-02*	13.70	0.58	0.85	12.82	0.54	0.70
LA-03	15.82	0.61	0.95	14.80	0.57	0.77
LA-04	15.27	0.56	0.90	14.28	0.53	0.73
Weighted mean	**15.52**	**0.41**	**0.83**	**14.52**	**0.39**	**0.64**
Aghla Beg RSF						
AB-01	16.32	0.95	1.21	15.26	0.89	1.04
AB-02	14.84	0.62	0.92	13.88	0.58	0.76
AB-03	15.75	0.72	1.02	14.73	0.67	0.85
Weighted mean	**15.44**	**0.42**	**0.83**	**14.45**	**0.39**	**0.65**
Muckish RSF						
MK-01	15.74	0.65	0.98	14.72	0.61	0.80
MK-03	16.27	0.61	0.97	15.22	0.57	0.78
MK-05*	14.39	0.56	0.87	13.46	0.52	0.70
Weighted mean	**16.02**	**0.45**	**0.86**	**14.99**	**0.42**	**0.67**
Slieve League RSF						
SL-02	16.84	0.69	1.04	15.75	0.64	0.85
SL-03	17.57	0.88	1.20	16.43	0.82	1.01
SL-04	16.87	0.85	1.15	15.77	0.79	0.97
Weighted mean	**17.04**	**0.46**	**0.91**	**15.94**	**0.43**	**0.71**

* 'Outlier' ages that differ at $p < 0.05$ from others from the same site; these are excluded from calculation of the uncertainty-weighted mean ages. Scaling from CRONUS online calculator (Balco *et al.,* 2008): wrapper script version 2.2; main calculator version 2.1; constants version 2.2.1; muons version 1.1. Internal uncertainties (±1σ) are analytical uncertainties on ^{10}Be measurements only. Total uncertainties (±1σ) incorporate in addition uncertainties in the calibration and scaling procedure.

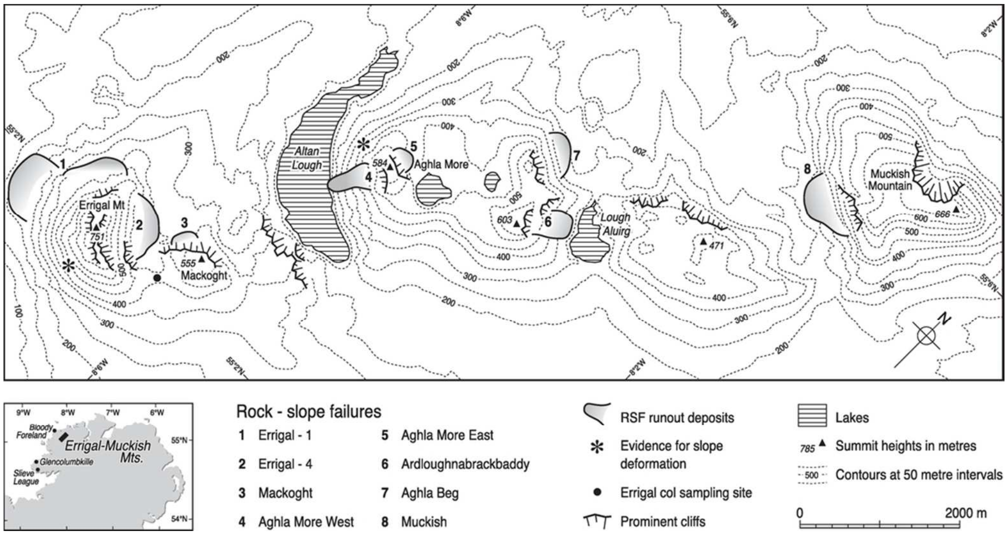

Location of sampled RSFs and the Errigal col sampling site in the Errigal-Muckish mountains. The outlying Slieve League RSF site is not shown.
93x49mm (300 x 300 DPI)

Figure 2. Donegal RSFs. (a) Hummocky runout debris of the Errigal-4 RSF. Mackoght is the peak to right of centre, with RSF runout debris just above the small lake at the base of the talus. (b) RSF debris lobe at Aghla More East. (c) Muckish RSF showing quarried frontal slope. (d) Slieve League RSF.
119x90mm (300 x 300 DPI)

Figure 3. (a-c) sampled boulders in RSF runout zones. (a) Sample LA-04. (b) Sample MGHT-02; the survey pole has 20 cm divisions. (c) Sample AB-02. (d) Glacially-plucked quartzite outcrops on the Errigal col, which were sampled to obtain deglaciation age.
120x91mm (300 x 300 DPI)

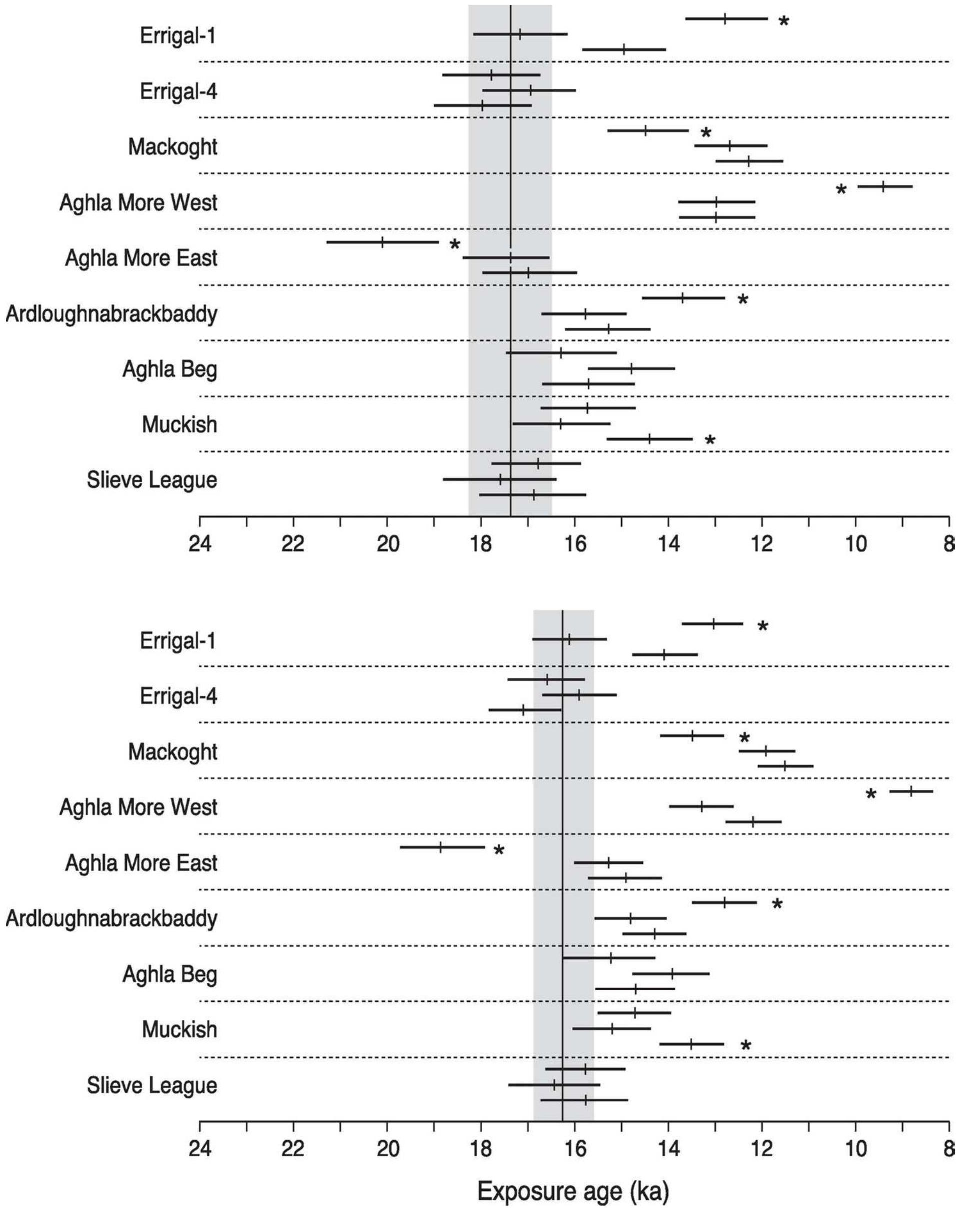

Figure 4. Exposure ages obtained for all RSF samples (vertical dashes); horizontal bars represent ± 1σ external uncertainties. Top: ages calculated using LL LPR. Bottom: ages calculated using NWH11.6 LPR. The vertical line represents the uncertainty-weighted mean deglaciation age for the Errigal col, and the shaded area represents the associated ± 1σ external uncertainty. Asterisked (*) ages are anomalous outliers that differ at $p < 0.05$ from other ages obtained at the same site. Note that Slieve League site was deglaciated much earlier, at ~19.1 ka (LL LPR).
128x162mm (300 x 300 DPI)

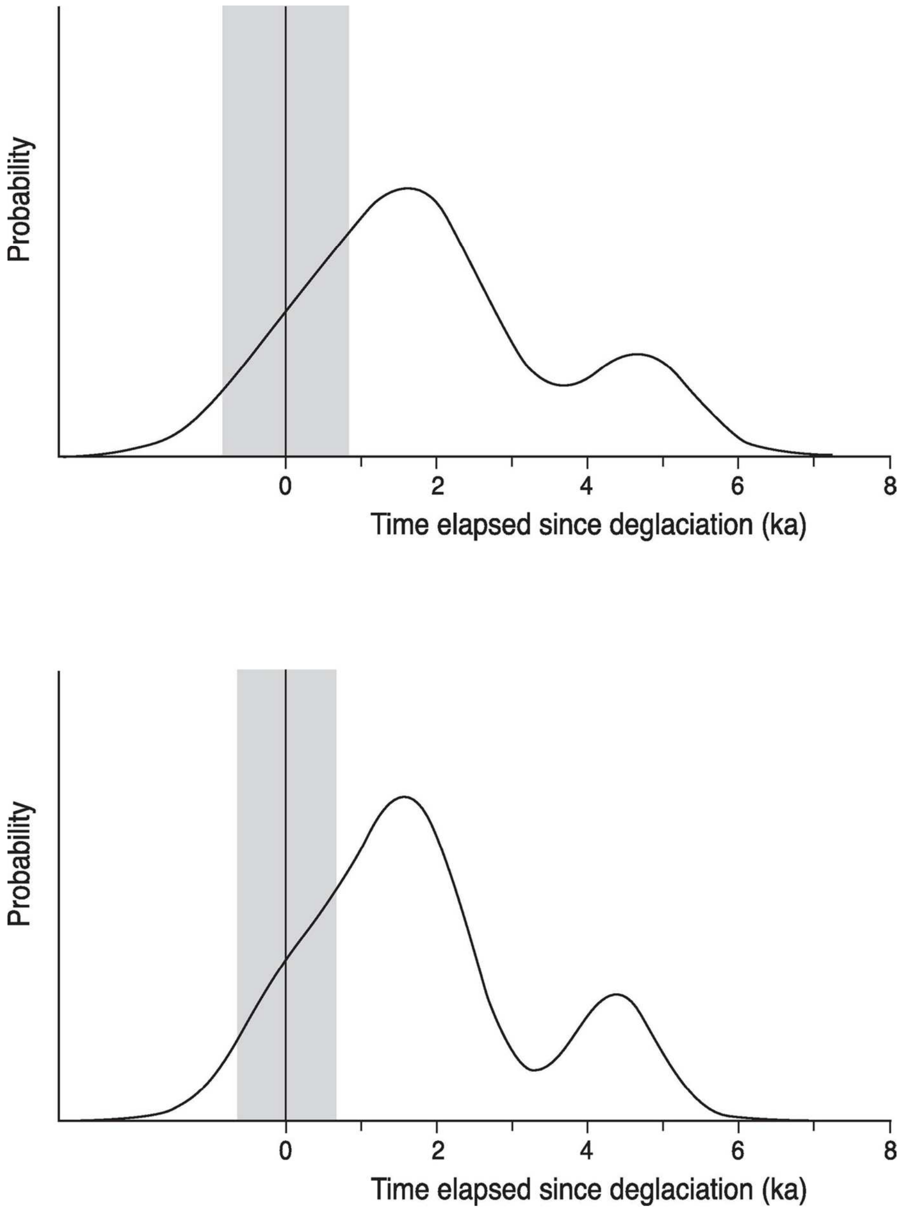

Figure 5. Probability density distributions of all RSF ages, calculated as time elapsed since deglaciation (t = 0). Top: calculated using LL LPR. Bottom: calculated using NHW11.6 LPR. Shaded zone represents deglaciation age (t = 0) ± 1σ uncertainty. The area under the curve left of t = 0 is a function of the calculation of probability density, which incorporates both weighted means and associated uncertainties. The differing shapes of the two curves reflect the greater uncertainties associated with the LL LPR age calibration (Table 2).
113x152mm (300 x 300 DPI)

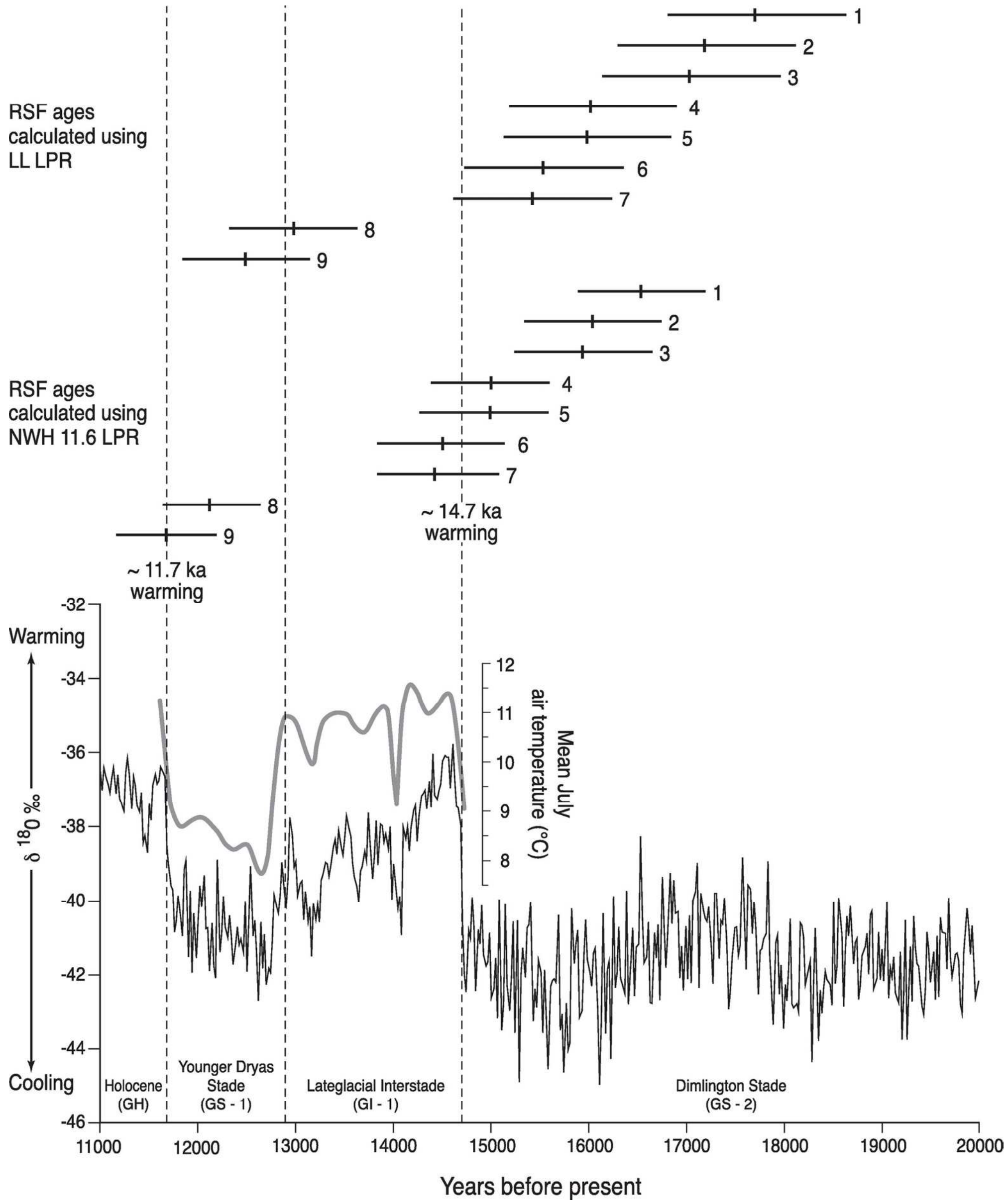

Figure 6. Weighted mean ages (vertical dashes) and associated ± 1σ external uncertainties for the nine dated RSFs plotted against deglaciation age, NGRIP ice core δ18O data for 12–21 ka (Rasmussen et al., 2006), the ice core stages proposed by Lowe et al. (2008) and mean July temperature data inferred from chironomid assemblages in SE Scotland (Brooks and Birks, 2000), matched to the NGRIP ice core data. 1: Errigal-4. 2: Aghla More East. 3: Slieve League. 4: Errigal-1. 5: Muckish. 6: Ardloughnabrackbaddy. 7: Aghla Beg. 8: Aghla More West. 9: Mackoght.
156x188mm (300 x 300 DPI)